

Basin-Scale Hydrologic Characterization of the La Dore Basin

Ali Haghghi

Surface Water Hydrology

Dr. Afshin Ashrafzadeh

February 11, 2026



Abstract

This report was prepared for the Master's Surface Hydrology course taught by Dr. Afshin Ashrafszadeh (Fall 2025). The analysis is based on CAMELS-FR, a catchment-scale hydrologic dataset for France that provides standardized basin attributes, meteorological forcings, and discharge time series; from CAMELS-FR, the La Dore basin at Saint-Gervais-sous-Meymont (station code K287191001; area 795 km²) was selected as a case study. We characterize basin physiography (morphometry, stream network, hypsometry), hydroclimate and runoff behavior (daily and monthly precipitation, discharge, and potential evapotranspiration; flow duration curve), and the long-term water balance for 1990–2020. Mean annual precipitation is about 1055 mm/yr, runoff 381 mm/yr, and the runoff ratio is 0.36. The project codebase is available at github.com/Alioax/hydro; the codebase includes hooks for remote-sensing products (GPM IMERG, SMAP) to support future extensions, and a planned end-of-report discussion will outline possible research directions building on this workflow.

1 Introduction

Basin-scale hydrologic characterization provides essential context for water-resources assessment, flood and low-flow analysis, and interpretation of runoff-generation processes. Using standardized datasets and a consistent workflow makes it possible to compare catchments objectively, communicate key hydrologic signatures, and establish a baseline for subsequent model development or the integration of remote-sensing products. This report builds on the CAMELS-FR dataset [1, 2].

In this report, the project includes:

- Basin physiography and drainage structure (morphometry, stream network, hypsometry).
- Hydroclimate and runoff behavior from CAMELS-FR time series.
- Water balance (annual and seasonal): precipitation, runoff, PET, residual.

Study scope. This report uses the CAMELS-FR dataset and SRTM DEM for one focus basin (La Dore, station K287191001). IMERG and SMAP remote-sensing products are not used in the present analysis; they are reserved for future work.

2 Study Area

2.1 Location and Boundary

The study basin is La Dore at Saint-Gervais-sous-Meymont (station code K287191001), with a catchment area of 795 km² and an outlet elevation of 398 m a.s.l. The outlet gauge (monitoring station) is located roughly 100 km west of the city of Lyon. Figure 1 shows the catchment boundary and gauge outlet on a basemap.

The basin lies in the Massif Central (France); coordinates at the outlet are approximately 3.61°E, 45.69°N (WGS84). It is one of the CAMELS-FR basins with area 500–1000 km² (see Appendix A). The climate is temperate oceanic with continental

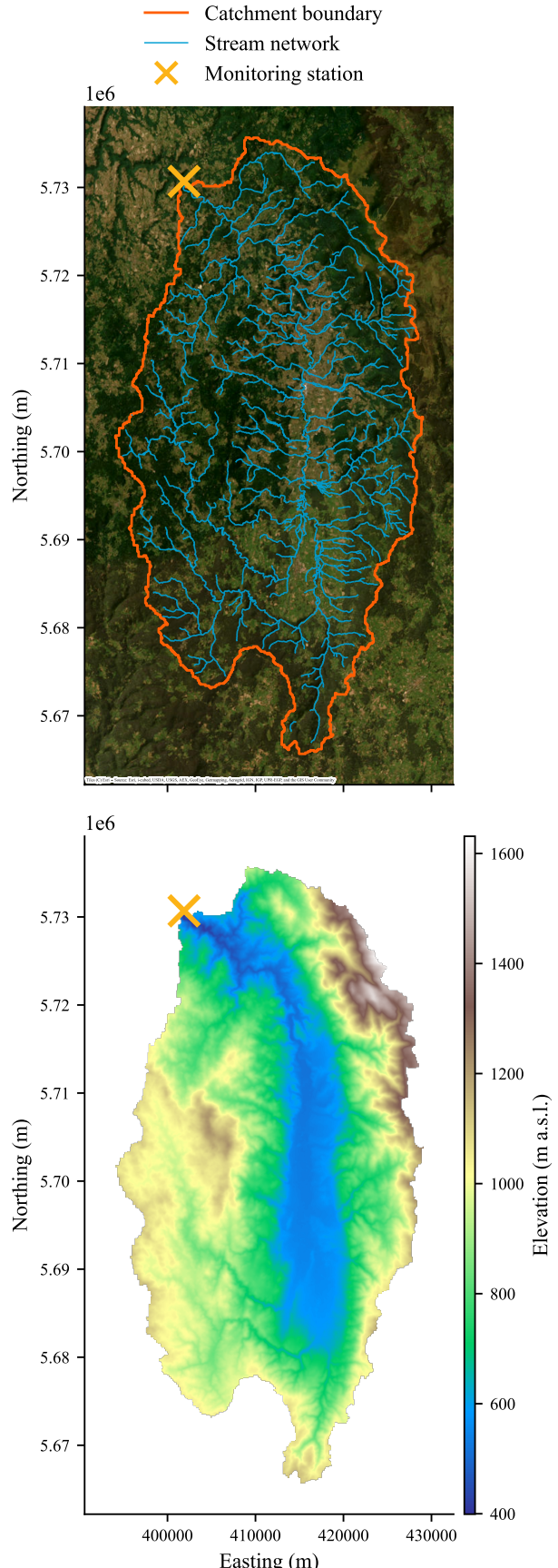


Figure 1: Catchment boundary and gauge outlet for station K287191001 (La Dore à Saint-Gervais-sous-Meymont). Area 795 km²; outlet elevation 398 m a.s.l. The stream network displayed is from an OpenStreetMap-derived stream product. Map displayed in Web Mercator (EPSG:3857).

tal influence; precipitation and runoff exhibit marked seasonality (winter–spring high flows, summer low flows).

3 Data Sources

3.1 CAMELS-FR

This project uses the CAMELS-FR large-sample hydrology dataset for France [1, 2]. CAMELS-FR provides catchment boundaries and gauge locations, standardized catchment attributes (e.g., basin area, elevation and relief, slopes, drainage-network and shape indices), and hydro-meteorological time series including precipitation, air temperature, potential evapo-transpiration, and discharge.

In this report, CAMELS-FR is used to (a) define the study basin and its boundary/outlet, (b) extract basin physiographic descriptors for the morphometric summary, and (c) supply the daily/monthly time series used for hydroclimate characterization, the flow-duration curve, and the 1990–2020 water-balance analysis. CAMELS-FR also provides a companion set of standardized graphical fact sheets for each basin; see Appendix B for the fact sheet for La Dore and an at-a-glance summary with additional basin details.

3.2 Terrain Data (SRTM DEM)

SRTM DEM (30 m) is used to derive terrain, drainage structure, and elevation-area relationships. GPM IMERG [3] and SMAP [4] are available for future extension (precipitation bias, soil moisture) but are not used in this report.

3.3 Analysis Period and Data Screening

Unless stated otherwise, the analysis period is 1990–2020 for the water balance and flow-duration curve, while the time-series snippet uses 2017–2020. Days with missing or invalid discharge are dropped; monthly aggregates use only months with at least 90% valid days.

4 Exploratory Analyses

This class project is organized as a set of exploratory analyses. For each analysis, we briefly summarize the workflow and then report the key outputs.

4.1 Basin Physiography and Drainage Structure

Workflow. Basin boundary and outlet are taken from CAMELS-FR geography (catchment boundaries and gauge outlet .gpkg). Basin terrain metrics and hypsometry are derived from SRTM DEM.

The stream network shown in Figure 1 is taken from an OpenStreetMap-derived stream product (not delineated in this project). We attempted to delineate streams from the DEM using pysheds [5] with D8 flow direction and flow accumulation; however, the extracted network and main channel were not satisfactory despite extensive debugging. As a result, we used the existing stream product for visualization. A priority for future work is to diagnose and fix the DEM-based delineation (e.g., preprocessing, sinks/breaching, burn-in, pro-

jection/resolution consistency, and threshold selection) so the stream network can be generated reproducibly from the DEM.

Outputs. Figure 1 provides a plan-view overview (boundary, drainage, and outlet gauge). Table 1 summarizes basin geometry, elevation, slope, shape, and drainage metrics.

Table 1: Basin physiography and morphometric metrics for La Dore (K287191001).

Metric	Value
Area (km ²)	795.0
Perimeter (km)	188.2
Basin length (km)	31.8
Main channel length (km)	22.98
Elevation min (m a.s.l.)	398
Elevation mean (m a.s.l.)	855
Elevation max (m a.s.l.)	1643
Relief (m)	1249
Outlet elevation (m a.s.l.)	398
Mean slope (degrees)	8.48
Compactness coefficient	1.88
Circularity ratio	0.28
Drainage density (km ⁻¹)	0.6548

4.2 Hypsometry and Altimetry

Workflow. The elevation distribution is summarized using the cumulative area–elevation (altimetric) curve. DEM pixels within the La Dore basin are sorted by elevation; the cumulative area at each elevation is computed as the area of all pixels at or below that elevation. The classic hypsometric curve is the same relationship expressed in normalized coordinates: normalized cumulative area (0–1) versus normalized elevation $(z - z_{\min})/(z_{\max} - z_{\min})$. The hypsometric integral is the area under the normalized curve.

Outputs. Figure 2 shows the cumulative area–elevation curve with both raw and normalized axes (top axis: normalized cumulative area; right axis: normalized elevation). The hypsometric integral is 0.37, indicating that the basin area is biased toward lower elevations. Most of the basin area lies between about 400 and 1200 m a.s.l.

4.3 Hydroclimate and Runoff Behavior

Workflow. We summarize variability at daily scale using a short multi-year snippet and at seasonal scale using monthly climatology. Runoff behavior is further summarized with a flow-duration curve (daily Q , 1990–2020).

Flow-duration curve. The flow-duration curve (FDC; Figure 5) uses all valid daily discharge values from 1990–2020 (no seasonal stratification), expressed as basin-normalized runoff depth (mm/day). To construct the FDC, daily values are pooled, missing/invalid discharge is removed, and the remaining values are sorted from largest to smallest. Each ranked value $Q_{(i)}$ is assigned an exceedance probability (percent of time flow is equaled or exceeded), computed as

$$p_i = 100 \times \frac{i}{N+1},$$

where i is the rank ($i = 1$ is the largest flow) and N is the

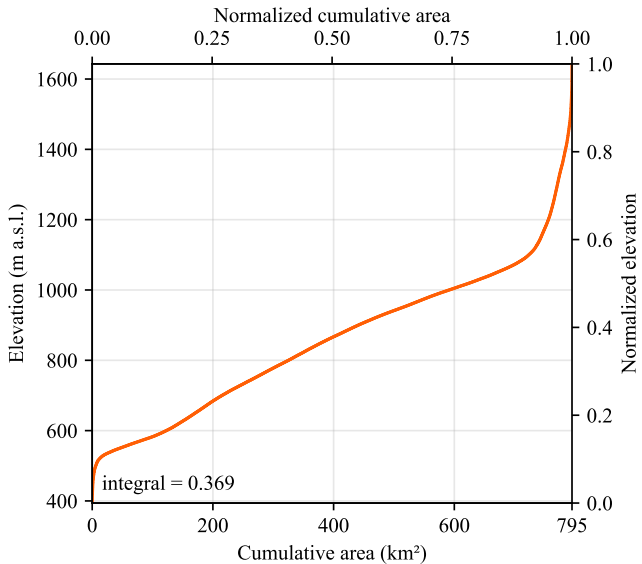


Figure 2: Altimetric (cumulative area–elevation) curve for La Dore. Bottom/left axes show cumulative area (km^2) and elevation (m a.s.l.); top/right axes show the same curve in normalized coordinates (0–1). The hypsometric integral (≈ 0.37) is the area under the normalized curve.

number of valid daily values. The curve then plots $Q_{(i)}$ against p_i ; discharge is shown on a logarithmic axis to resolve both high flows (small exceedance) and low flows (near-perennial exceedance) on the same panel.

Interpretation. In Figure 5, the upper tail (small exceedance percentages) is steep, indicating that the largest flows occur relatively infrequently and drop off quickly—consistent with event-driven peaks superimposed on a seasonal regime. The mid-portion of the curve is comparatively smooth, suggesting a persistent range of typical flows rather than abrupt switching between wet and dry states. The lower tail approaches a small but nonzero discharge (order-of-magnitude 10^{-1} mm/day), implying perennial behavior with low flows generally maintained, likely supported by catchment storage/baseflow. Approximate read-offs from the curve place the median daily runoff near $\sim 1 \text{ mm/day}$, while low-flow conditions (e.g., exceedance $\sim 90\%$) are on the order of a few 10^{-1} mm/day . Overall, the FDC complements Figures 3–4 by quantifying how frequently different parts of the flow regime occur, separating rare high-flow behavior from the more persistent baseflow/typical-flow regime.

Outputs. Figure 3 compiles daily discharge, basin-average rainfall, potential evapotranspiration (PET), and air temperature for 2017–2020 on a common time axis. Temperature and PET show a strong annual cycle (winter minima and summer maxima), with PET reaching order-of-magnitude $\sim 4\text{--}5 \text{ mm/day}$ in summer. This seasonal atmospheric demand provides context for the discharge regime: flows are generally higher and more persistent during the cool season, while extended low-flow periods dominate during the warm season when PET is high.

Rainfall occurs throughout the year as intermittent events, including occasional high-intensity days (peaks approaching

$\sim 60 \text{ mm}$). However, the discharge response to rainfall is modulated by season and antecedent wetness. During late autumn through spring, rainfall events often coincide with sharp runoff peaks and sustained elevated flow, suggesting relatively full catchment storage and efficient conversion of precipitation to streamflow. In contrast, during summer, even when rainfall occurs, discharge commonly remains low or responds weakly, consistent with larger soil-moisture deficits and stronger evaporative demand that reduces effective precipitation and limits runoff generation. Prolonged recession periods following wet-season peaks highlight the role of catchment storage and groundwater contributions in maintaining baseflow between events.

Figure 4 summarizes the monthly climatology (multi-year monthly means) of precipitation (P), discharge/runoff (Q), and PET. Precipitation remains comparatively high across much of the year (roughly $\sim 65\text{--}110 \text{ mm/month}$), with an enhancement from late spring through autumn. In contrast, PET peaks strongly in the warm season: it is minimal in winter (single digits to low teens mm/month), rises rapidly in spring, and reaches maxima in early–mid summer (order-of-magnitude $\sim 100+ \text{ mm/month}$), before declining again in autumn.

The discharge climatology follows the combined influence of P and PET rather than precipitation alone. Highest Q occurs in the cool season (approximately Jan–Mar and again in late autumn/early winter), when PET is low and a larger fraction of precipitation becomes effective rainfall, allowing catchment storage to remain high and sustain runoff. Through late spring and summer, Q decreases steadily to a clear late-summer minimum, despite precipitation remaining substantial in some months, indicating that high PET and associated soil-moisture deficits suppress runoff generation.

Viewed as a seasonal partitioning, the figure highlights three regimes: (i) winter surplus ($P \gg \text{PET}$) with the highest runoff and runoff efficiency (Q/P); (ii) summer deficit ($\text{PET} \gtrsim P$) with the lowest runoff; and (iii) an autumn transition when PET declines while P remains high, promoting catchment rewetting and recovery of Q toward winter levels. Figure 5 shows the flow-duration curve.

4.4 Water Balance

Workflow. We use the long-term water-balance identity $P - Q - \text{PET} \approx \Delta S$, where ΔS is interpreted as a residual that combines storage change and data/model uncertainty. The runoff ratio is Q/P . We summarize annual totals and long-term means for 1990–2020.

Annual water-balance aggregation. Annual precipitation (P) and potential evapotranspiration (PET) were computed as the sum of daily basin-average values for each calendar year. Annual runoff (Q) was computed by converting daily mean discharge to an equivalent basin-depth (mm/day) using the catchment area and summing across the year to obtain mm/yr . The plotted residual is

$$R = P - Q - \text{PET}.$$

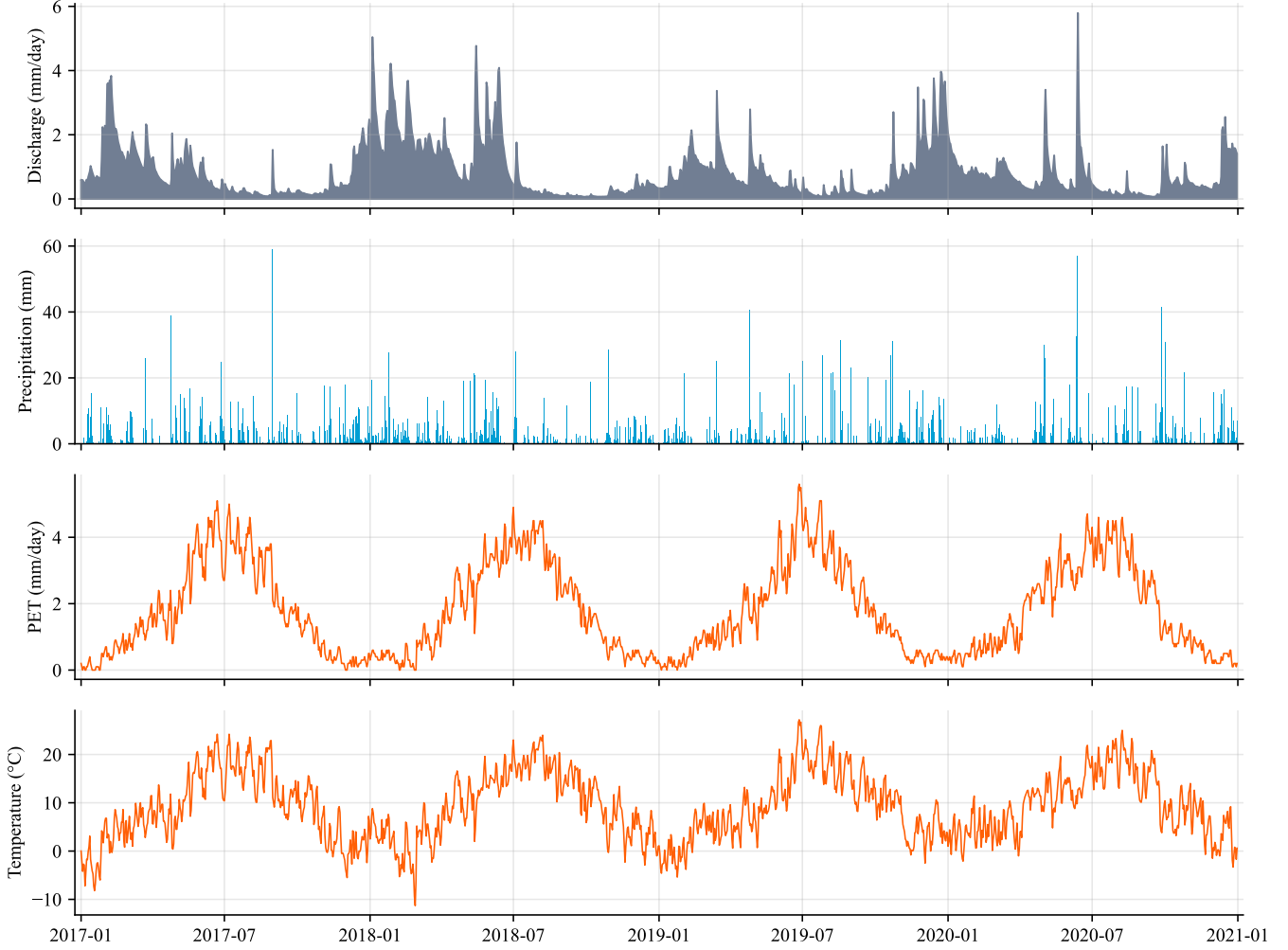


Figure 3: Daily discharge, rainfall, potential evapotranspiration (PET), and air temperature for 2017–2020. The synchronized panels highlight strong seasonality in temperature and PET (summer maxima, winter minima) and show that higher, more sustained flows occur predominantly in the cool season when PET is low, whereas warm-season high PET coincides with extended low flows and generally muted runoff responses to rainfall events.

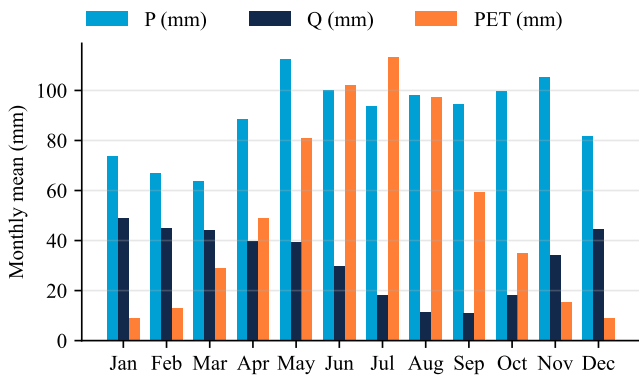


Figure 4: Monthly climatology of precipitation (P), discharge (Q), and potential evapotranspiration (PET). PET increases sharply from spring to a summer maximum, coinciding with a pronounced reduction in Q , while cool-season low PET aligns with the highest Q and greatest runoff efficiency, indicating strong seasonal control of streamflow by the balance between water inputs and atmospheric demand.

Because PET represents potential (atmospheric-demand-limited) evapotranspiration rather than actual evapotranspiration (ET), R should be interpreted as a combined term that can include changes in catchment storage (ΔS), differences between ET and PET, and forcing/measurement errors (e.g., precipitation undercatch, discharge uncertainty).

Outputs. Figure 6 summarizes the interannual water balance from 1990–2020 by comparing annual P , annual Q , annual PET, and the residual ($R = P - Q - PET$). Across the record, precipitation exhibits strong year-to-year variability, while PET is comparatively stable and primarily reflects climatic energy demand (smaller interannual swings than P). Runoff varies substantially and generally co-varies with P , indicating that wetter years tend to produce higher annual runoff, whereas drier years yield lower runoff totals.

The residual provides a compact diagnostic of whether annual precipitation is accounted for by runoff plus atmospheric demand. Positive residual years indicate that P exceeds $(Q + PET)$, consistent with conditions where some combination of (i) catchment storage increases (soil/groundwater recharge) and/or (ii) actual evapotranspiration is below PET

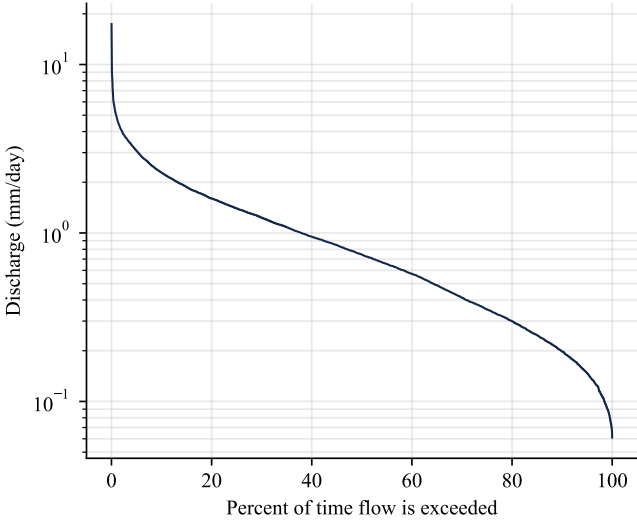


Figure 5: Flow-duration curve of daily discharge (1990–2020). Daily Q values (mm/day; basin-normalized) are ranked from highest to lowest and plotted against exceedance probability p (percent of time flow is equaled or exceeded; $p_i = 100i/(N+1)$). Discharge is plotted on a logarithmic axis to emphasize both high-flow and low-flow behavior.

(water-limited ET). Negative residual years indicate that $(Q + PET)$ exceeds P , which can occur when stored water from prior wet periods is released (net storage drawdown), when actual ET approaches/exceeds the PET proxy used, or when input/output uncertainties are non-negligible. For this reason, the residual should be interpreted qualitatively—as an indicator of storage/closure behavior and potential data/forcing inconsistencies—rather than a direct estimate of storage change alone.

Long-term means (1990–2020) are: $P \approx 1055 \text{ mm/yr}$, $Q \approx 381 \text{ mm/yr}$, $\text{PET} \approx 592 \text{ mm/yr}$, runoff ratio $Q/P \approx 0.36$, and residual $\approx 82 \text{ mm/yr}$ ($\sim 8\%$ of P).

5 Future Research

Runoff in La Dore is controlled by seasonal precipitation and PET (higher Q in winter–spring, lower in summer), by the basin’s moderate slopes and drainage density, and by storage (soil moisture, possibly snow). A runoff ratio of 0.36 is within the range typical for temperate, mid-elevation catchments. Limitations include single-gauge discharge, reanalysis-based P and PET, and the use of PET rather than actual ET. The following subsections outline promising directions for future research.

5.1 Hydrological Modeling and Scenario Analysis

An immediate extension is to implement a rainfall–runoff model for the La Dore basin to deepen process understanding and enable scenario testing. Thus far, analysis has been empirical; introducing a calibrated hydrological model (e.g., a conceptual model like GR4J or similar) would allow simulation of streamflow under varied conditions. This would illuminate the basin’s runoff sensitivity to changes in precipitation or

evapotranspiration, and enable experiments such as adjusting inputs to mimic climate change or land-use shifts. Such modeling aligns with the CAMELS-FR dataset’s aim of supporting model benchmarking across basins, and would yield quantitative insight into how the moderate-relief La Dore might respond to extreme events or future climatic variability. Ultimately, a model provides a predictive tool to complement the descriptive analyses, refining our ability to attribute changes in flow regimes to specific drivers.

5.2 Integration of Satellite Precipitation Data

Another promising direction is to leverage high-resolution satellite precipitation estimates (e.g., NASA’s GPM IMERG) to validate and enhance the basin’s precipitation inputs. Gauge-based rainfall data, while reliable at a point, may miss spatial variability in the catchment, especially during convective storms. IMERG offers near-global coverage and has shown generally strong agreement with European gauge-based datasets ($R^2 \sim 0.8$). By comparing IMERG rainfall with ground observations over La Dore, one can identify biases or under-catch issues and improve the water balance closure. Moreover, incorporating IMERG as an additional forcing or for bias-correction could sharpen analysis of extreme events (e.g., intense rainfalls leading to floods) by providing better spatial and temporal resolution. Care must be taken in areas of complex terrain (IMERG can underestimate precipitation in mountains), but given La Dore’s moderate relief, satellite data integration is a feasible step to strengthen precipitation assessment and ensure the robustness of runoff calculations.

5.3 Leveraging Satellite Soil Moisture for Runoff Dynamics

The availability of SMAP soil moisture data opens an opportunity to investigate subsurface conditions and their influence on runoff. Antecedent soil moisture is a known control on flood generation, yet the current study inferred it only indirectly through long-term balance. By using SMAP (which provides near-surface soil moisture observations), future work can examine how wetness levels prior to rainfall affect stream responses. Recent research demonstrates that runoff generation in small basins exhibits threshold behavior that is captured only when combining antecedent soil moisture with rainfall metrics. Applying this concept, one could analyze La Dore’s rainfall–runoff events to determine critical soil saturation thresholds for runoff initiation, improving flood predictability. Additionally, SMAP data can be assimilated or compared with modelled soil moisture, serving as an independent check on hydrological model states. Studies have shown that satellite-derived moisture correlates well with deeper storage changes and can help validate model simulations of root-zone soil moisture and groundwater dynamics. Incorporating SMAP thus offers a way to link surface observations with subsurface processes in the basin, refining our understanding of infiltration, storage, and baseflow generation under temperate

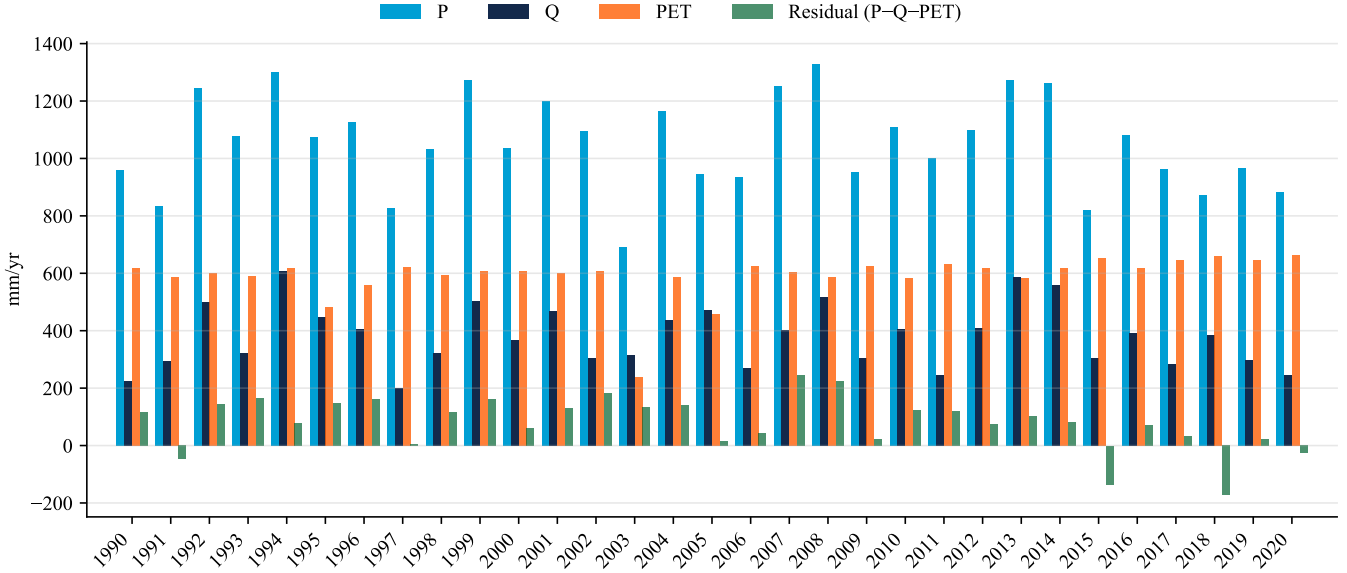


Figure 6: Annual water-balance components (1990–2020): precipitation (P), runoff (Q) (basin-normalized), and potential evapotranspiration (PET) (all in mm/yr). The residual is $R = P - Q - PET$. Because PET is potential (not actual) evapotranspiration, R represents a combined closure term that may include storage change, ET–PET differences, and forcing/measurement uncertainty.

conditions.

5.4 Cross-Basin Comparative Analysis

Finally, situating the La Dore findings within a broader regional context would add significant value. A single basin’s behavior can be idiosyncratic; cross-comparing La Dore with other French catchments (especially the 654 minimally disturbed basins in CAMELS-FR) can reveal whether its hydrological patterns are general or unique. By examining metrics like runoff ratios, flow duration characteristics, or seasonality across similar temperate basins, one could identify how factors such as geology or relief contribute to differences in water response. This comparative approach aligns with the ethos of large-sample hydrology—no single watershed captures the full diversity of hydrologic behavior—and helps assess the generality of conclusions drawn from La Dore. It could also involve testing a hydrological model trained on La Dore against neighboring basins to evaluate model transferability. Overall, multi-basin analysis would strengthen the study by highlighting broader hydroclimatic patterns and ensuring that insights from La Dore are placed in the context of regional hydrology and long-term change. Each basin comparison or grouping could uncover systematic trends (or anomalies) that single-basin analysis might overlook, providing a richer foundation for future hydrological investigations.

6 Conclusion

We characterized the La Dore basin (795 km^2) using CAMELS-FR and SRTM DEM. Mean annual precipitation is about 1055 mm/yr, runoff 381 mm/yr, and the runoff ratio is 0.36, with strong seasonality (winter–spring high flows, summer low flows). The analysis provides a baseline for hydrological modeling, satellite integration, and cross-basin comparison.

References

- [1] Olivier Delaigue et al. *CAMELS-FR dataset*. Version V3. 2024. doi: [10.57745/WH7FJR](https://doi.org/10.57745/WH7FJR). URL: <https://doi.org/10.57745/WH7FJR>.
- [2] Olivier Delaigue et al. “CAMELS-FR dataset: a large-sample hydroclimatic dataset for France to explore hydrological diversity and support model benchmarking”. In: *Earth System Science Data* 17.4 (2025), pp. 1461–1479. doi: [10.5194/essd-17-1461-2025](https://doi.org/10.5194/essd-17-1461-2025). URL: <https://doi.org/10.5194/essd-17-1461-2025>.
- [3] G. J. Huffman et al. *GPM IMERG Final Precipitation L3 1 day 0.1 degree × 0.1 degree V07 (GPM_3IMERGDF)*. Subset: Baton Rouge, Louisiana, 2022–2024. Accessed 2025-09-27. Greenbelt, Maryland, USA, 2023. doi: [10.5067/GPM/IMERGDF/DAY/07](https://doi.org/10.5067/GPM/IMERGDF/DAY/07). URL: <https://data.nasa.gov/dataset/gpm-imerg-final-precipitation-l3-1-day-0-1-degree-x-0-1-degree-v07-gpm-3imergdf-at-ges-dis-13ed8>.
- [4] P. E. O’Neill et al. *SMAP Enhanced L3 Radiometer Global and Polar Grid Daily 9 km EASE-Grid Soil Moisture, Version 6*. Subset: Baton Rouge, Louisiana, 2022–2024. Accessed 2025-09-27. Boulder, Colorado USA, 2021. doi: [10.5067/M200XIZHY3RJ](https://doi.org/10.5067/M200XIZHY3RJ). URL: https://nsidc.org/data/SPL3SMP_E.
- [5] Matt Bartos. *pysheds: simple and fast watershed delineation in python*. 2020. doi: [10.5281/zenodo.3822494](https://doi.org/10.5281/zenodo.3822494). URL: <https://github.com/mdbartos/pysheds>.
- [6] Olivier Delaigue et al. *CAMELS-FR graphical fact sheets*. Version V1. 2024. doi: [10.57745/KK2SVJ](https://doi.org/10.57745/KK2SVJ). URL: <https://doi.org/10.57745/KK2SVJ>.

A CAMELS-FR basins with catchment area 500–1000 km²

The following 77 basins from the CAMELS-FR dataset have catchment area between 500 and 1000 km² and an outlet gauge. Station code: Hydroportail `sta_code_h3`. Sorted by catchment area.

Column definitions. Outlet alt. is the elevation (m.a.s.l.) of the gauge at the catchment outlet. Mean flow is mean annual runoff (mm/yr). **Agr. (agriculture)** is the percentage of the catchment area classified as agricultural land (CORINE Land Cover 2018, level 1), aggregated to the catchment.

#	Area	Code	Station (river at location)	Period	Out. alt (m)	Mean flow (mm/yr)	Agr. (%)
1	500.1	A975201001	La Nied [Française] à Condé-Northen [Pontigny]	1968-11-01–present	202	227.9	75.9%
2	502.2	A369011001	La Sauer à Beinheim	1964-10-23–present	114	219.4	23.6%
3	506.0	Y503201001	L'Argens à Châteauvert	1971-07-01–present	179	209.2	25.4%
4	508.0	M123304010	La Braye à Sargé-sur-Braye	1990-05-01–present	87	192.8	85.0%
5	512.9	M313301010	La Varenne à Saint-Fraimbault [Moulin Crinais]	1991-06-01–present	112	466.5	86.6%
6	524.3	O234401001	Le Girou à Cépet	1968-09-01–present	120	142.9	92.9%
7	542.5	X043401001	L'Ubaye à Barcelonnette [Abattoir]	1904-01-01–present	1134	577.0	4.5%
8	544.8	O787401001	Le Dourdou [de Conques] à Conques	1974-11-01–present	239	404.9	64.6%
9	548.9	H032103001	L'Ource à Autricourt	1966-12-31–present	196	353.2	43.4%
10	558.8	F415000101	L'Ouanne à Charny	1968-06-01–present	136	200.3	73.2%
11	561.5	L440000101	La Petite Creuse à Genouillac	1967-01-01–present	278	296.5	84.6%
12	562.6	K337301001	La Bouble à Chareil-Cintrat	1966-07-01–present	244	200.8	77.8%
13	568.3	L510181001	La Garonne à Folles [Pont Gibus]	1960-01-01–present	282	433.2	65.1%
14	574.9	K565301001	L'Auron à Bourges - L'Ormeiot	1966-12-19–present	128	184.3	76.3%
15	575.7	J474201001	L'Ellé à Arzano - Ty Nadan [aval pont]	1969-01-01–present	19	525.5	80.3%
16	584.4	O509252002	L'Aveyron à Onet-le-Château	1967-12-31–present	531	332.9	61.6%
17	586.8	V605201001	L'Ouvèze à Vaison-la-Romaine	1971-02-03–present	194	320.6	26.9%
18	589.9	U221502001	Le Dessoubre à Saint-Hippolyte	1955-06-01–present	383	725.2	58.6%
19	593.4	K117321001	L'Arconce à Montceaux-l'Étoile	1969-12-01–present	244	290.2	80.9%
20	599.3	J795301020	Le Don à Guémené-Penfao - Juzet	1979-12-18–present	10	200.6	89.7%
21	607.6	H640203001	La Vesle à Puisieulx	1983-09-01–present	85	136.4	76.0%
22	609.4	U092402001	La Vingeanne à Oisilly	1970-12-01–present	196	313.3	72.2%
23	616.5	K633252001	La Saône à Brion-sur-Saône	1987-06-01–present	128	224.8	77.9%
24	618.0	H506201001	Le Rognon à Doulaincourt-Saucourt	1968-08-01–present	204	484.6	49.0%
25	622.1	A330010001	La Moder à Schweighouse-sur-Moder [aval]	1966-05-11–present	143	267.1	29.3%
26	626.9	A420063001	La Moselle à Saint-Nabord - Noirgueux	1961-10-30–present	362	1192.1	22.5%
27	628.6	H612201001	L'Aire à Varennes-en-Argonne	1968-08-01–present	155	442.3	73.9%
28	646.8	0001004003	La Garonne à Saint-Béat - HE	1992-01-01–present	507	1093.2	1.0%
29	647.8	H020302002	La Laignes aux Riceys	1983-12-01–present	177	156.1	61.6%
30	662.4	K077322001	Le Lignon à Poncins - Le Bourg	1966-01-01–present	332	365.2	47.9%
31	668.5	A116003002	L'Ill à Didenheim	1973-10-04–present	242	300.7	59.7%
32	673.0	H512234001	L'Ornain à Tronville-en-Barrois	1988-12-01–present	205	379.7	55.3%
33	675.2	Y604201001	Le Var à Entrevaux [Pont-levis]	1920-01-01–present	475	665.4	3.1%
34	677.5	0811351001	Le Célé à Figeac [Merlançon]	1937-01-01–2005-01-01	182	591.4	63.0%
35	684.0	0359402002	Le Dourdou [de Camarès] à Vabres-l'Abbaye - Le Poujol	1987-09-03–present	300	490.2	42.6%
36	686.0	H010002001	La Seine à Plaines-Saint-Lange	1967-08-01–present	180	501.5	54.4%
37	696.4	V177401001	La Bourbre à Tignieu-Jameyzieu	1909-01-01–present	203	338.1	68.0%
38	704.5	U233401001	L'Allan à Fesches-le-Châtel	1986-06-03–present	319	468.4	34.7%
39	722.4	Y028406001	Le Tech à Argelès-sur-Mer - Pont d'Elne	1984-08-30–present	9	359.3	17.5%
40	727.1	A615103001	La Meurthe à Raon-l'Étape	1973-11-01–present	282	604.1	24.2%
41	731.7	M377181010	L'Odon à Châtelais [Marcillé]	1972-09-01–present	29	180.0	93.5%
42	734.9	A907105050	La Sarre à Diedendorf	1970-07-01–present	220	320.0	49.5%

continued on next page

continued from previous page

#	Area	Code	Station (river at location)	Period	Out. alt (m)	Mean flow (mm/yr)	Agr. (%)
43	751.1	H774201001	Le Therain à Beauvais	1967-12-31-present	66	226.9	80.6%
44	772.3	K125181001	L'Arroux à Dracy-Saint-Loup [Surmoulin]	1984-02-01-present	289	253.9	72.4%
45	791.8	Q219252001	La Midouze [Le Midou] à Mont-de-Marsan	1967-01-01-2011-03-14	36	283.3	70.0%
46	792.0	E550572001	L'Authie à Dompierre-sur-Authie	1963-01-01-present	10	308.3	88.1%
47	795.0	K287191001	La Dore à Saint-Gervais-sous-Meymont [Maison du Parc/Giroux-Dore]	1919-01-01-present	398	408.9	34.8%
48	798.1	U464401001	L'Azergues à Lozanne	1964-11-17-present	198	272.3	60.0%
49	809.2	J748301001	La Seiche à Bruz - Carcé	1967-11-21-present	16	181.8	89.7%
50	810.4	H631302001	La Suisse à Orainville	1968-01-15-present	57	159.2	82.4%
51	816.6	M711241010	La Sèvre Nantaise à Tiffauges - Ancienne Station	1967-10-01-present	49	361.0	91.3%
52	832.5	M036151010	L'Huisne à Nogent-le-Rotrou [Pont de bois]	1971-11-17-present	106	237.9	76.0%
53	845.0	U122401001	La Tille à Arceau [Arcelot]	1966-07-01-present	222	267.4	47.6%
54	851.5	F453000101	L'Essonne à Guigneville-sur-Essonne - La Mothe	1974-04-01-present	54	141.5	77.8%
55	852.0	U104401001	L'Ognon à Chassey-lès-Montbozon [Bonnal]	1986-12-09-present	248	618.7	37.7%
56	853.3	L441171001	La Petite Creuse à Fresselines [Puy Rageaud]	1924-01-01-present	222	297.2	84.7%
57	860.7	K518302002	La Tardes à Évaux-les-Bains	1921-01-01-2008-06-01	385	317.7	82.8%
58	868.0	H425042010	L'Avre à Muzy	1971-05-01-present	80	127.5	73.9%
59	876.2	Q028003001	L'Adour à Estirac	1968-10-01-present	165	558.0	43.1%
60	877.3	F416000201	L'Ouanne à Gy-les-Nonains	1968-11-22-present	103	177.1	76.9%
61	881.8	U122402001	La Tille à Cessey-sur-Tille	1962-12-21-present	200	245.1	49.1%
62	882.7	I522101001	La Vire à Saint-Lô [Pont de Gourfaleur]	1969-09-01-present	14	447.8	91.8%
63	884.3	P638251001	L'Auvézère au Change [Aubarède]	1964-01-01-present	97	300.1	64.3%
64	886.3	L620201002	La Claise au Grand-Pressigny [Étableau 1] - Étableau 2	1976-12-31-2019-12-31	57	153.6	61.5%
65	909.5	M005061020	La Sarthe à Saint-Céneri-le-Gérei - Moulin-du-Désert	1977-12-01-present	122	241.1	82.3%
66	917.2	E540031001	La Canche à Brimeux	1962-01-01-present	4	414.6	86.2%
67	929.4	K538302101	L'Aumance à Hérisson - Pont de la Roche	1969-10-01-2008-07-16	181	236.8	88.0%
68	934.2	F467000101	L'Orge à Morsang-sur-Orge	1967-01-01-present	40	130.6	44.3%
69	937.8	U342401001	La Seille à Saint-Usuge	1968-03-01-present	178	458.0	62.5%
70	939.9	P392252001	La Corrèze à Brive-la-Gaillarde - Pont du Buy	1900-01-01-present	107	683.1	43.5%
71	943.2	X045401001	L'Ubaye au Lauzet-Ubaye [Roche-Rousse]	1959-10-01-present	798	674.3	5.2%
72	944.9	0314101001	Le Tarn à Mostuéjouls [La Muse]	1912-12-31-present	398	921.0	10.4%
73	948.1	A543101001	Le Madon à Pulligny	1964-01-01-present	223	333.3	77.0%
74	954.2	P392252002	La Corrèze à Brive-la-Gaillarde - Le Prieur	1918-01-01-2016-02-22	101	662.6	43.1%
75	956.9	H616201001	L'Aire à Chevières	1960-01-01-present	118	430.0	72.0%
76	987.8	U303401001	La Dheune à Palleau	1990-10-01-present	175	231.3	63.1%
77	994.0	K259301001	L'Alagnon à Lempdes-sur-Allagnon	1968-01-01-present	432	378.4	47.6%

B CAMELS-FR graphical fact sheet for basin K287191001

Figure 7 is taken from the CAMELS-FR graphical fact sheets dataset, which provides a standardized one-page fact sheet (with the same type of figure and layout) for each basin in CAMELS-FR [6].

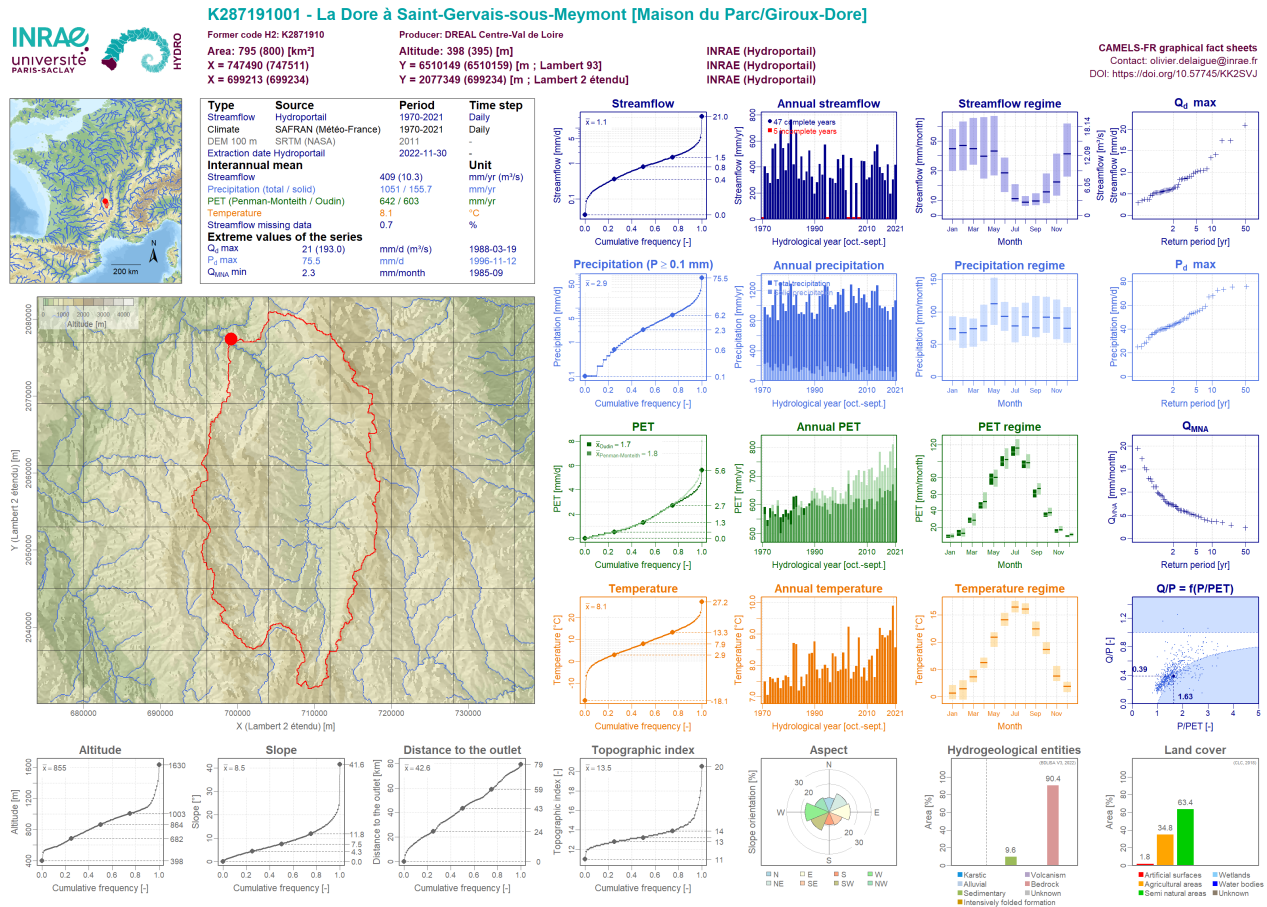


Figure 7: CAMELS-FR graphical fact sheet for La Dore at Saint-Gervais-sous-Meymont (station code K287191001), reproduced from the CAMELS-FR graphical fact sheets dataset [6].